Journal of Materials Chemistry A

RSC Publishing

PAPER

View Article Online
View Journal | View Issue

Cite this: *J. Mater. Chem. A*, 2013, **1**, 12635

High-efficiently visible light-responsive photocatalysts: Ag_3PO_4 tetrahedral microcrystals with exposed {111} facets of high surface energy†

Binjie Zheng, Xue Wang, Chang Liu, Kai Tan,* Zhaoxiong Xie* and Lansun Zheng

Received 29th July 2013
Accepted 23rd August 2013

DOI: 10.1039/c3ta12946b

www.rsc.org/MaterialsA

In this article, single-crystalline tetrahedral Ag_3PO_4 microcrystals with exposed {111} facets was successfully synthesized *via* a facile wet chemical method. The tetrahedral Ag_3PO_4 with exposed {111} facets showed the highest photocatalytic activity in visible light irradiation among the {111}, {110} and {100} facets. By DFT calculations, it is demonstrated that the surface energy of the {111} facets is higher than that of the {110} and {100} facets. It was found that the largest band gap of the Ag_3PO_4 {111} surface is likely to suppress the recombination of electron–hole pairs by exploring the electronic structures of the different surfaces of Ag_3PO_4. Meanwhile, the dispersion between the valence bands and conduction bands of the {111} surface is beneficial for the separation of photogenerated electrons and holes on the {111} surface, which further improves the photocatalytic activity of the {111} surface.

Introduction

The utilization of solar energy has been attracting more and more attention, and the search for new photocatalysts for the utilization of solar energy has been prevalent in the past decades.[1–10] At present, many wide band gap semiconductors, such as TiO_2, have been demonstrated to be excellent photocatalysts in the fields of photodegradation and water splitting.[11,12] However, due to their wide band gap, only ultraviolet (UV) light, which is less than 4% of the solar spectrum, can be used in the process of photocatalytic reactions. Therefore, the development of visible light-responsive photocatalysts is becoming more and more important. Besides extending the light absorption to the visible light region by the doping of wide band gap materials,[13,14] exploring new visible light-responsive photocatalysts has aroused growing research interest recently. Ag_3PO_4, with a band gap of 2.36 eV, is a newly developed photocatalyst, showing excellent high photocatalytic activity in the degradation of organic dyes under visible light irradiation and high photo-oxidative capability for O_2 evolution from water.[8,15–24]

From the viewpoint of photocatalysis, the photocatalytic activity not only depend on the composition of the materials, but also depends on the surface structure of the materials.[25,26] In particular, recent studies have shown that crystalline photocatalysts, with higher energy crystal facets, usually exhibit better activities, which has stimulated researchers to synthesize crystalline photocatalysts with higher energy crystal facets.[27–33] For example, numerous efforts have been paid to the synthesis of anatase TiO_2 with high energy {001} facets, and it has been demonstrated that the {001} facets exhibit excellent photodegeneration activity.[28,34,35] For the new catalyst Ag_3PO_4, Ye's group demonstrated that high energy {110} facets of Ag_3PO_4 exhibited much higher photocatalytic activity than low energy {100} facets.[15] Therefore, improving the photocatalytic activity by the control of surface structures is important and necessary. In this article, we report a facile route for synthesizing single-crystalline tetrahedral Ag_3PO_4 microcrystals with {111} facets exposed, which are of higher surface energy than those of the {110} and {100} facets. Tetrahedral Ag_3PO_4 with exposed {111} facets showed extremely high visible light photocatalytic activity. In addition, first-principle density functional theory (DFT) calculations were carried out for a deep understanding of the photocatalytic activities of the different crystal facets.

Experimental

Synthetic methods

Synthesis of Ag_3PO_4 tetrahedra. 43 mg silver nitrate was dissolved in 2 mL ethanol, and then the solution was slowly dropped into 10 mL 0.1 M H_3PO_4 ethanol solution (stirring with a magnet at a rotation speed of 300 rpm). The process was performed in a water bath kept at 60 °C. The obtained yellow

State Key Laboratory of Physical Chemistry of Solid Surfaces & Department of Chemistry, College of Chemistry and Chemical Engineering, Xiamen University, Xiamen 361005, China. E-mail: zxxie@xmu.edu.cn; ktan@xmu.edu.cn; Fax: +86-592-2183047; Tel: +86-592-2180627

† Electronic supplementary information (ESI) available: histogram of particle size distributions of the Ag_3PO_4 tetrahedral microcrystals; XRD patterns of RD and cubic Ag_3PO_4; SEM images and Zeta potentials of tetrahedral, RD and cubic Ag_3PO_4; TEM characterization of tetrahedral Ag_3PO_4; adsorption properties of MB, MO and RhB over Ag_3PO_4 tetrahedra, RD and cubes under dark conditions; pseudo first-order reaction kinetics of MB, MO and RhB over Ag_3PO_4 tetrahedra, RD and cubes. See DOI: 10.1039/c3ta12946b

precipitate was washed with ethanol several times and dried under vacuum.

Synthesis of Ag_3PO_4 rhombic dodecahedra (RD). Ag_3PO_4 rhombic dodecahedra and cubes were prepared by a method similar to that reported by Ye *et al.*[15] 100 mg silver acetate was dissolved in 80 mL distilled water, then 0.15 M Na_2HPO_4 aqueous solution was dropped into the above solution. The process was performed in a water bath kept at 60 °C. The obtained yellow precipitate was washed with water several times and dried under vacuum.

Synthesis of Ag_3PO_4 cubes. 100 mg silver nitrate was dissolved in 10 mL distilled water. 0.1 M ammonia solution was added to form a transparent solution, and the total volume of the solution was brought to 80 mL by adding distilled water. Then, 0.15 M Na_2HPO_4 aqueous solution was dropped into the above solution. The process was performed in a water bath kept at 30 °C. The obtained yellow precipitate was washed with water several times and dried under vacuum.

Characterization

Powder X-ray diffraction (XRD) patterns were recorded using a Panalytical X-pert diffractometer with copper Kα irradiation. Scanning electron microscopy (SEM, Hitachi S-4800) was employed to investigate the morphology of the as-prepared samples. The TEM samples were prepared by depositing a drop of the diluted suspension in distilled water on a copper grid coated with a carbon film. Because the Ag_3PO_4 particles can be easily reduced to Ag particles in high-resolution transmission electron microscopy (HRTEM, JEM 2100) with an high accelerating voltage of 200 kV, the morphology and crystal structure of the as-prepared products were observed by transmission electron microscopy (TEM, JEM 1400) with an accelerating voltage of 100 kV. UV-visible diffuse reflectance spectroscopy (DRS) was carried out with a Varian Cary-5000 UV-vis-NIR spectrophotometer. The Zeta potentials were detected on a Malvern Nano-ZS.

Photoreactivity measurements

In all of the photocatalytic activity experiments, the samples (10 mg) were made into an 80 mL aqueous solution (containing 1 μmol dye) and stirred in the dark for 20 min. Then the solution was irradiated with a 500 W Xenon lamp equipped with an ultraviolet cutoff filter to provide visible light with $\lambda \geq 420$ nm. The degradation of organic dyes was monitored by UV-vis spectroscopy (UV-2550, Shimadzu). Before the spectroscopy measurements, the photocatalysts were removed by centrifugation.

Theoretical calculations

The electronic structure calculations were based on the density functional theory (DFT)+U approach.[36] The exchange-correlation energy functional was represented by the local-density approximation (LDA).[37] Projector-augmented wave pseudopotentials were employed as implemented in the CASTEP code.[38] The valence configurations of the pseudopotentials are $4d^{10}5s^1$ for Ag, $2s^22p^4$ for O and $3s^23p^3$ for P. The energy cutoff for the plane wave basis set is 300 eV, and a Monkhorst–Pack k-mesh of $4 \times 4 \times 4$ was used for a 16-atom unit cell of cubic Ag_3PO_4 (space group $P\bar{4}3n$). The obtained lattice constant from LDA+U was $a = 5.89$ Å. The relaxed unit cell was used to construct the surface models. In the case of the (100) surface, a 32-atom slab model was created by extending the 16-atom unit cell along the z-direction by a factor of two. It was then expanded by 2×2 in the xy plane to construct the 128-atom supercell. For the other faces, the stoichiometric slab models were kept at a total of 128 atoms and the vacuum region had the same thickness (15 Å) as Ag_3PO_4. These surface structures were fully relaxed to a force convergence of 0.05 eV $Å^{-1}$, where the second layer was fixed to represent a bulk region. Based on the geometry relaxations, the surface energy (γ) was computed using the formula:[39]

$$\gamma = \frac{E_{slab} - nE_{bulk}}{2A}$$

where E_{slab} is the total energy of the slab, E_{bulk} is the total energy of the bulk per unit cell, n is the number of bulk unit cells contained in the slab, and A is the exposed area of one side of the slab.

Results and discussion

Ag_3PO_4 tetrahedrons with exposed {111} facets were synthesized by a simple reaction between silver nitrate–ethanol solution and H_3PO_4–ethanol solution at 60 °C. Fig. 1a shows the typical powder X-ray diffraction (XRD) pattern of the product, which can be indexed to the pure body-centered-cubic (bcc) structure of Ag_3PO_4 with cell constants of $a = 6.013$ Å (JCPDS no. 06-0505). The scanning electron microscopy (SEM) image shows that the products consist of Ag_3PO_4 tetrahedra with average sizes of 0.52 μm (Fig. S1†) in a high yield (Fig. 1b and S2†). The TEM image and corresponding SAED pattern (Fig. S3†) of the tetrahedra

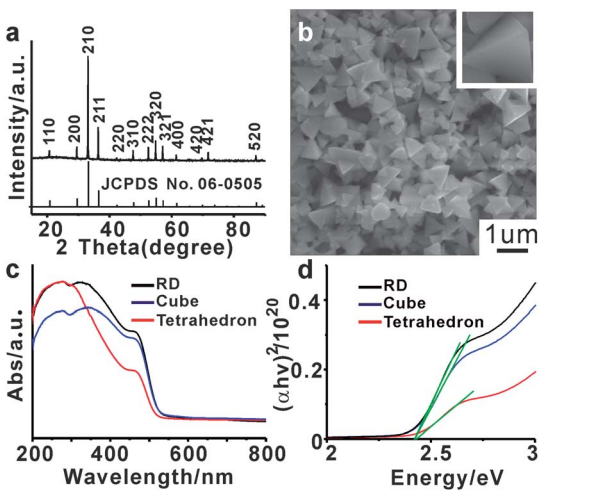

Fig. 1 (a) XRD patterns of the tetrahedral Ag_3PO_4 sub-microcrystals. (b) SEM images of the tetrahedral Ag_3PO_4 sub-microcrystals. (c) Ultraviolet-visible diffusive reflectance spectra of the tetrahedral, rhombic dodecahedral and cubic Ag_3PO_4 microcrystals. (d) Plot of $(\alpha h\nu)^2$ *vs.* photon energy ($h\nu$) for the determination of the direct optical band gap of the tetrahedral, rhombic dodecahedral and cubic Ag_3PO_4 microcrystals.

indicate that the as-prepared Ag_3PO_4 particles are single crystalline and the exposed surfaces of the tetrahedra are {111} facets. The UV-vis diffuse reflectance spectra (Fig. 1c) reveal that the Ag_3PO_4 tetrahedral particles could absorb visible light with wavelengths shorter than 516 nm. The direct optical band gap E_g of the Ag_3PO_4 tetrahedra was determined to be 2.43 eV (Fig. 1d) from the equation listed below:[40]

$$\alpha h\nu = A(h\nu - E_g)^{1/2}$$

where α is the absorption coefficient and A is a constant. The absorption coefficient α was calculated from k (extinction coefficient) using $\alpha = 4\pi k/\lambda$. For comparison, the rhombic dodecahedral (RD) Ag_3PO_4 microcrystals with exposed {110} facets (Fig. S4a†) and cubic Ag_3PO_4 microcrystals exposed with {100} facets (Fig. S4b†) were synthesized by a method similar to that reported by Ye *et al.*,[15] and the optical properties of RD and cubic Ag_3PO_4 were also investigated under visible light irradiation. As shown in Fig. 1c and d, the RD and cubic Ag_3PO_4 microcrystals could absorb visible light with a wavelength shorter than 520 nm, and the direct optical band gaps E_g of the RD and cubic Ag_3PO_4 were both determined to be 2.42 eV.

It is known that the photocatalytic activity of materials not only depends on the bulk structure, but also on the surface structure, and different surfaces may exhibit different photocatalytic activity. From the XRD patterns of the three types of Ag_3PO_4 (Fig. 1c and S5†), we can not see any difference in crystallinity. In addition, the direct optical band gaps (E_g) of the three types of Ag_3PO_4 are very similar, therefore we focus on the surface effects of the three Ag_3PO_4 photocatalysts. In order to investigate the surface effects on the photocatalytic activity, the photocatalytic performance of the tetrahedral, RD and cubic Ag_3PO_4 micro-crystallites under visible light irradiation was studied. In the photocatalytic experiments, positively charged methylene blue (MB) was used for the photodecomposition experiments. As shown in Fig. 2a, tetrahedral Ag_3PO_4 with exposed {111} facets exhibited the highest photocatalytic activity in the degradation of MB, while cubic Ag_3PO_4 with exposed {100} facets exhibited the lowest photocatalytic activity. Due to the negatively charged surfaces of the three types of Ag_3PO_4 (Fig. S6†), one may think that the good photocatalytic activity was attributed to the adsorption between the samples with negative charge and the MB with positive charge. Therefore, negatively charged methyl orange (MO) and neutral rhodamine B (RhB) were also used as probe molecules to investigate the photocatalytic performance of the three types of Ag_3PO_4 under visible light irradiation. As shown in Fig. 2b and c, tetrahedral Ag_3PO_4 with exposed {111} facets still showed the highest photocatalytic activity in the degradation of MO and RhB, while cubic Ag_3PO_4 with exposed {100} facets exhibited the lowest photocatalytic activity. Additionally, by analysing the photodegeneration with a pseudo first-order reaction, the absolute rate constant value of tetrahedral Ag_3PO_4 is higher than that of RD and cubic Ag_3PO_4 in the degradation of MB, MO and RhB (Fig. S7†), which further indicates the highest photocatalytic activity of tetrahedral Ag_3PO_4. Meanwhile, in order to avoid the effect of the adsorption abilities of the different crystal facets, the adsorption curves of MB, MO and RhB over tetrahedra, rhombic dodecahedra and cubes under dark conditions were also measured. It was found that the adsorption abilities of the tetrahedra, rhombic dodecahedra and cubes towards MB, MO and RhB are very weak (Fig. S8, S9 and S10†). Therefore, the highest photocatalytic activity of tetrahedral Ag_3PO_4 with exposed {111} facets is attributed to the degradation ability of the catalysts, and the photocatalytic activities of the Ag_3PO_4 crystal surfaces were in the order of {111} > {110} > {100}.

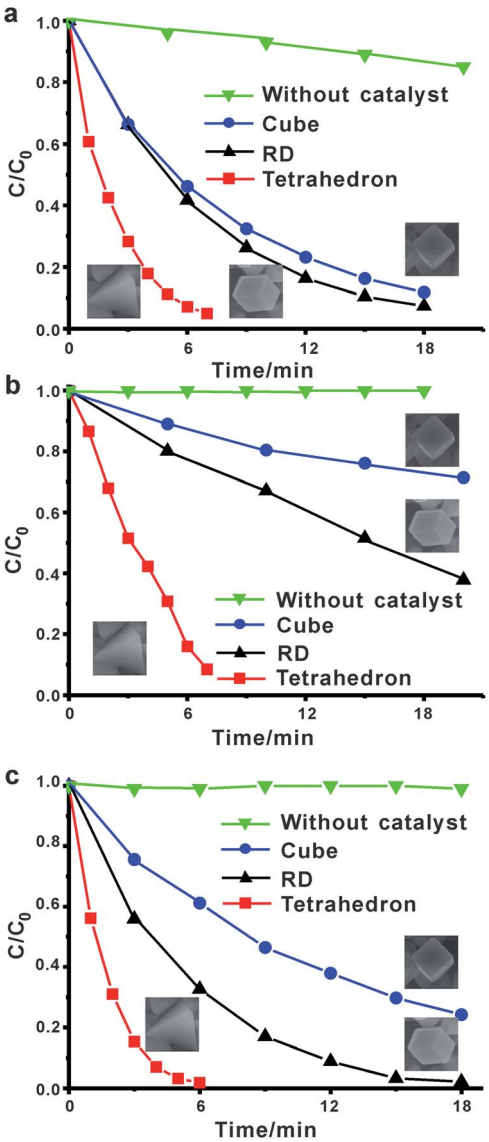

Fig. 2 Photocatalytic activity of the Ag_3PO_4 rhombic dodecahedra, cubes and tetrahedra for (a) MB, (b) MO and (c) RhB degradation under visible light irradiation ($\lambda \geq 420$ nm).

It is known that the photodegradation of organic pollutants is a surface oxidation process, which is driven by photogenerated electron–hole pairs correlated with the surface structure. Therefore, for the photocatalytic behaviour of semiconductors, the most crucial factor is the chemical adsorption and reaction of target molecules occurring on the surface of

semiconductors. To clarify the surface effect on the photocatalytic properties of the Ag_3PO_4 photocatalysts, the surface energies of the Ag_3PO_4 {111}, {110} and {100} facets were calculated by first-principle density functional theory (DFT). The relaxed unit cells used to construct models of the Ag_3PO_4 (111), (110) and (100) surfaces are shown in Fig. 3. For each face, the surface model is constructed on the basis of a slab model including 128 atoms of Ag_3PO_4 with a vacuum region of the same thickness as Ag_3PO_4. The calculated results show that the surface energy of the Ag_3PO_4 (111) surface is estimated to be 1.65 J m^{-2}, which is obviously higher than that of Ag_3PO_4 (110) (1.31 J m^{-2}) and Ag_3PO_4 (100) (1.10 J m^{-2}). This result also indicates that the {111} facets are more active than the {110} and {100} facets, and provide higher photocatalytic activity for the degradation of organic dyes in visible light irradiation, which explains the photocatalytic results in Fig. 2.

Moreover, to further study the relationship between the Ag_3PO_4 surface and the photocatalytic activity, it is important to explore the electronic structures of the different surfaces of Ag_3PO_4. Although the band gap from DFT calculations is usually underestimated, they often provide important insight into the physicochemical behavior of the materials investigated.[41] Scissors of 2.0 eV were employed for the results analysis. Fig. 4 shows the energy-band structure of Ag_3PO_4 calculated using CASTEP. The band structure of bulk Ag_3PO_4 is shown in Fig. 4a, and the direct band gap of bulk Ag_3PO_4 is 2.48 eV at the *G* point. Unlike the band structure of bulk Ag_3PO_4, the band gaps of the Ag_3PO_4 {111}, {110} and {100} surfaces are 2.736 eV, 2.613 eV and 2.032 eV, respectively. The highest band gap of the Ag_3PO_4 {111} surface is likely to suppress the recombination of electron–hole pairs, and thus accounts for the highest photooxidative activity. Furthermore, it is important to note that the bottoms of the conduction bands of the Ag_3PO_4 {111}, {110} and {100} surfaces are 2.735 eV, 2.610 eV and 1.920 eV, respectively. Therefore, the photogenerated electrons on the Ag_3PO_4 {111} surface possess higher energy and activity than those on the {110} and {100} surfaces.

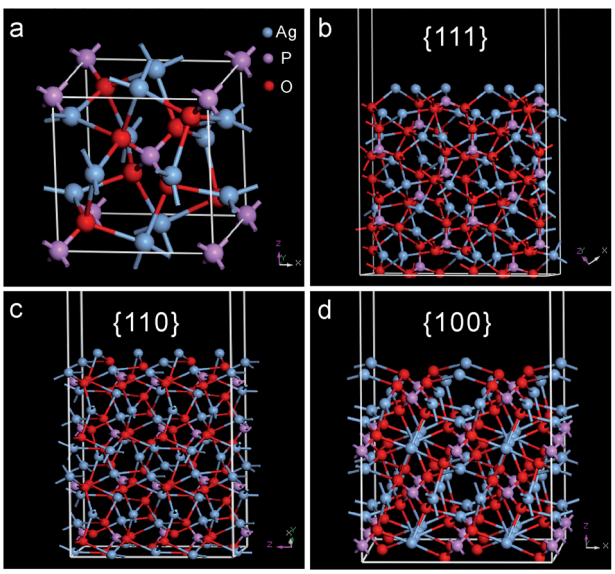

Fig. 3 (a) The crystal structure of Ag_3PO_4; relaxed geometries for the (b) (111), (c) (110) and (d) (100) surfaces of Ag_3PO_4 based on a 128-atom slab model. The vacuum region was set as the same thickness as Ag_3PO_4.

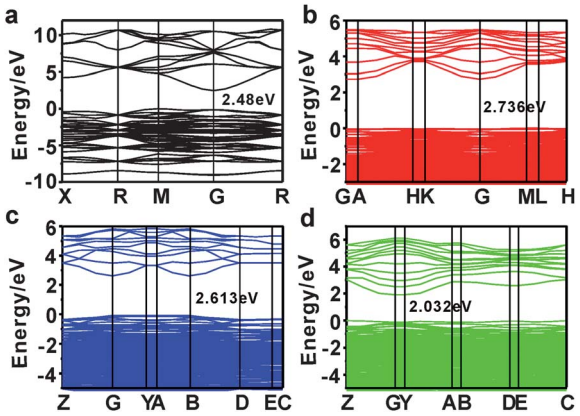

Fig. 4 Energy-band structures of Ag_3PO_4: (a) bulk phase, and the (b) {111}, (c) {110} and (d) {100} surfaces of Ag_3PO_4.

To further elucidate the composition and the nature of the electronic band structures, the total density of states (TDOS) of Ag_3PO_4 and the partial DOS (PDOS) for s, p and d orbitals are calculated, as shown in Fig. 5. As reported previously, the bottoms of the conduction bands are mainly composed of hybridized Ag 5s5p as well as a small quantity of P 3s orbitals, whereas the tops of the valence bands are composed of hybridized Ag 4d and O 2p orbitals.[8] However, by analysing the PDOS of the Ag_3PO_4 {111}, {110} and {100} surfaces in detail, we find that the component of the s orbitals emerges at an energy band at about −0.11 eV for the {100} surface and −0.26 eV for the {110} surface. The s orbitals are mainly contributed by Ag 5s orbitals and narrow the band gap of the {110} and {100} surfaces. More specifically, compared with the {110} surface, with the {100} surface, the s orbitals can easier pass through the Fermi energy level, leading to the metal-like electronic properties of Ag_3PO_4 {100} surface, which results in the easier recombination between the photogenerated electrons and holes.[16]

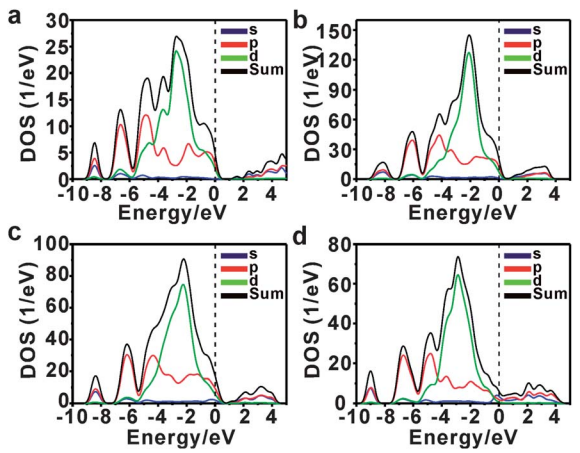

Fig. 5 Total DOS and partial DOS of Ag_3PO_4: (a) bulk phase, and the (b) {111}, (c) {110} and (d) {100} surfaces of Ag_3PO_4.

However, no similar s orbitals appear near the Fermi energy level in the PDOS of the {111} surface. Hence, the dispersion between the valence bands and conduction bands is beneficial for the separation of photogenerated electrons and holes on the {111} surface, which further improves the photocatalytic activity of the {111} surface. The calculation results above further indicate that the Ag_3PO_4 {111} surface is the most active of the Ag_3PO_4 {111}, {110} and {100} surfaces, and the Ag_3PO_4 {100} surface is the least active, which is also consistent with the results in Fig. 2.

In summary, single-crystalline tetrahedral Ag_3PO_4 with exposed {111} facets was synthesized by simply reacting silver nitrate with H_3PO_4–ethanol solutions at 60 °C *via* a facile wet chemical method. Among the {111}, {110} and {100} facets, the tetrahedral Ag_3PO_4 with exposed {111} facets showed the highest photocatalytic activity in visible light irradiation. Meanwhile, the results of the DFT calculations showed that the surface energy of the {111} facets is higher than that of the {110} and {100} facets. By exploring the electronic structures of the different surfaces of Ag_3PO_4, the highest band gap for the Ag_3PO_4 {111} surface is likely to suppress the recombination of electron–hole pairs. Furthermore, the dispersion between the valence bands and conduction bands of the {111} surface is beneficial for the separation of photogenerated electrons and holes on the {111} surface, which further improves the photocatalytic activity of the {111} surface. The study above provides us with a method of improving the photocatalytic activity of materials, and motivates us to develop other visible light-sensitive photocatalysts by surface control.

Acknowledgements

This work was supported by the National Basic Research Program of China (Grant no. 2011CBA00508, 2013CB933901), the National Natural Science Foundation of China (Grant no. 21333008, 21131005, 21021061, and 21171141).

Notes and references

1 A. Fujishima and K. Honda, *Nature*, 1972, **238**, 37.
2 Z. G. Zou, J. H. Ye, K. Sayama and H. Arakawa, *Nature*, 2001, **414**, 625.
3 A. Ishikawa, T. Takata, J. N. Kondo, M. Hara, H. Kobayashi and K. Domen, *J. Am. Chem. Soc.*, 2002, **124**, 13547.
4 K. Maeda, K. Teramura, D. L. Lu, T. Takata, N. Saito, Y. Inoue and K. Domen, *Nature*, 2006, **440**, 295.
5 K. Awazu, M. Fujimaki, C. Rockstuhl, J. Tominaga, H. Murakami, Y. Ohki, N. Yoshida and T. Watanabe, *J. Am. Chem. Soc.*, 2008, **130**, 1676.
6 X. C. Wang, K. Maeda, A. Thomas, K. Takanabe, G. Xin, J. M. Carlsson, K. Domen and M. Antonietti, *Nat. Mater.*, 2009, **8**, 76.
7 J. H. Li and J. Z. Zhang, *Coord. Chem. Rev.*, 2009, **253**, 3015.
8 Z. G. Yi, J. H. Ye, N. Kikugawa, T. Kako, S. X. Ouyang, H. Stuart-Williams, H. Yang, J. Y. Cao, W. J. Luo, Z. S. Li, Y. Liu and R. L. Withers, *Nat. Mater.*, 2010, **9**, 559.
9 H. Wang, J. Gao, T. Q. Guo, R. M. Wang, L. Guo, Y. Liu and J. H. Li, *Chem. Commun.*, 2012, **48**, 275.
10 W. L. Yang, L. Zhang, Y. Hu, Y. J. Zhong, H. B. Wu and X. W. Lou, *Angew. Chem., Int. Ed.*, 2012, **51**, 11501.
11 X. B. Chen and S. S. Mao, *Chem. Rev.*, 2007, **107**, 2891.
12 A. Kudo and Y. Miseki, *Chem. Soc. Rev.*, 2009, **38**, 253.
13 R. Asahi, T. Morikawa, T. Ohwaki, K. Aoki and Y. Taga, *Science*, 2001, **293**, 269.
14 S. Sakthivel and H. Kisch, *Angew. Chem., Int. Ed.*, 2003, **42**, 4908.
15 Y. P. Bi, S. X. Ouyang, N. Umezawa, J. Y. Cao and J. H. Ye, *J. Am. Chem. Soc.*, 2011, **133**, 6490.
16 Y. P. Bi, H. Y. Hu, S. X. Ouyang, G. X. Lu, J. Y. Cao and J. H. Ye, *Chem. Commun.*, 2012, **48**, 3748.
17 Z. B. Jiao, Y. Zhang, H. C. Yu, G. X. Lu, J. H. Ye and Y. P. Bi, *Chem. Commun.*, 2013, **49**, 636.
18 H. Wang, Y. S. Bai, J. T. Yang, X. F. Lang, J. H. Li and L. Guo, *Chem.–Eur. J.*, 2012, **18**, 5524.
19 J. Wang, F. Teng, M. D. Chen, J. J. Xu, Y. Q. Song and X. L. Zhou, *CrystEngComm*, 2013, **15**, 39.
20 H. Y. Hu, Z. B. Jiao, H. C. Yu, G. X. Lu, J. H. Ye and Y. P. Bi, *J. Mater. Chem. A*, 2013, **1**, 2387.
21 P. Y. Dong, Y. H. Wang, H. H. Li, H. Li, X. L. Ma and L. L. Han, *J. Mater. Chem. A*, 2013, **1**, 4651.
22 Y. P. Bi, H. Y. Hu, Z. B. Jiao, H. C. Yu, G. X. Lu and J. H. Ye, *Phys. Chem. Chem. Phys.*, 2012, **14**, 14486.
23 H. Wang, L. He, L. H. Wang, P. F. Hu, L. Guo, X. D. Han and J. H. Li, *CrystEngComm*, 2012, **14**, 8342.
24 Q. H. Liang, W. J. Ma, Y. Shi, Z. Li and X. M. Yang, *CrystEngComm*, 2012, **14**, 2966.
25 Z. Y. Zhou, N. Tian, J. T. Li, I. Broadwell and S. G. Sun, *Chem. Soc. Rev.*, 2011, **40**, 4167.
26 Z. Y. Jiang, Q. Kuang, Z. X. Xie and L. S. Zheng, *Adv. Funct. Mater.*, 2010, **20**, 3634.
27 X. W. Xie, Y. Li, Z. Q. Liu, M. Haruta and W. J. Shen, *Nature*, 2009, **458**, 746.
28 H. G. Yang, C. H. Sun, S. Z. Qiao, J. Zou, G. Liu, S. C. Smith, H. M. Cheng and G. Q. Lu, *Nature*, 2008, **453**, 638.
29 M. Leng, M. Z. Liu, Y. B. Zhang, Z. Q. Wang, C. Yu, X. G. Yang, H. J. Zhang and C. Wang, *J. Am. Chem. Soc.*, 2010, **132**, 17084.
30 X. M. Zhou, J. Y. Lan, G. Liu, K. Deng, Y. L. Yang, G. J. Nie, J. G. Yu and L. J. Zhi, *Angew. Chem., Int. Ed.*, 2012, **51**, 178.
31 X. G. Han, M. S. Jin, S. F. Xie, Q. Kuang, Y. Q. Jiang, Z. Y. Jiang, Z. X. Xie and L. S. Zheng, *Angew. Chem., Int. Ed.*, 2009, **48**, 9180.
32 X. Wang, X. G. Han, S. F. Xie, Q. Kuang, Z. Y. Jiang, S. B. Zhang, X. L. Mu, G. X. Chen, Z. X. Xie and L. S. Zheng, *Chem.–Eur. J.*, 2012, **18**, 2283.
33 X. Wang, Z. Y. Jiang, B. J. Zheng, Z. X. Xie and L. S. Zheng, *CrystEngComm*, 2012, **14**, 7579–7582.
34 X. G. Han, Q. Kuang, M. S. Jin, Z. X. Xie and L. S. Zheng, *J. Am. Chem. Soc.*, 2009, **131**, 3152.
35 H. G. Yang, G. Liu, S. Z. Qiao, C. H. Sun, Y. G. Jin, S. C. Smith, J. Zou, H. M. Cheng and G. Q. Lu, *J. Am. Chem. Soc.*, 2009, **131**, 4078.
36 V. I. Anisimov, J. Zaanen and O. K. Andersen, *Phys. Rev. B: Condens. Matter Mater. Phys.*, 1991, **44**, 943.

37 J. P. Perdew and A. Zunger, *Phys. Rev. B: Condens. Matter Mater. Phys.*, 1981, **23**, 5048.
38 M. D. Segall, P. J. D. Lindan, M. J. Probert, C. J. Pickard, P. J. Hasnip, S. J. Clark and M. C. Payne, *J. Phys.: Condens. Matter*, 2002, **14**, 2717.
39 X. Q. Gong, A. Selloni, M. Batzill and U. Diebold, *Nat. Mater.*, 2006, **5**, 665.
40 M. A. Butler, *J. Appl. Phys.*, 1977, **48**, 1914.
41 J. J. Liu, X. L. Fu, S. F. Chen and Y. F. Zhu, *Appl. Phys. Lett.*, 2011, **99**, 191903.